Geophysical Research Letters

RESEARCH LETTER
10.1029/2021GL092465

Key Points:

- We use deep learning algorithms to identify nearly 100 swarms in Southern California lasting 6 months to 7 years
- 53% of the swarms have ultra-slow diffusive patterns with propagating backfronts, suggesting they are fluid driven
- The chronology of the swarms shows that these aseismic driving processes were occurring at all times during 2008–2020

Supporting Information:

Supporting Information may be found in the online version of this article.

Correspondence to:

Z. E. Ross,
zross@caltech.edu

Citation:

Ross, Z. E., & Cochran, E. S. (2021). Evidence for latent crustal fluid injection transients in Southern California from long-duration earthquake swarms. *Geophysical Research Letters*, *48*, e2021GL092465. https://doi.org/10.1029/2021GL092465

Received 11 JAN 2021
Accepted 26 MAY 2021

Evidence for Latent Crustal Fluid Injection Transients in Southern California From Long-Duration Earthquake Swarms

Zachary E. Ross[1] **and Elizabeth S. Cochran**[2]

[1]Seismological Laboratory, California Institute of Technology, Pasadena, CA, USA, [2]Earthquake Science Center, U.S. Geological Survey, Pasadena, CA, USA

Abstract Earthquake swarms are manifestations of aseismic driving processes deep in the crust. We examine the spatiotemporal distribution of aseismic processes in Southern California using a 12-years catalog of swarms derived with deep learning algorithms. In a core portion of the plate boundary region, which is not associated with elevated heat flow, we identify 92 long-duration swarms ranging from 6 months to 7 years that constitute 26.4% of the total seismicity. We find that 53% of the swarms exhibit ultra-slow diffusive patterns with propagating backfronts, consistent with expectations for natural fluid injection processes. The chronology of the swarms indicates that the aseismic driving processes were active at all times during 2008–2020. The observations challenge common views about the nature of swarms, which would characterize any one of these sequences as anomalous. The regional prevalence of these sequences suggests that transient fluid injection processes play a key role in crustal fluid transport.

Plain Language Summary Earthquake swarms are one of the main types of earthquake sequences. In contrast to mainshock-aftershock sequences, swarms are believed to be driven predominantly by processes other than tectonic loading or earthquake interactions. We build a high resolution catalog of earthquakes using machine learning algorithms to study long-duration swarms and their physical driving processes. We find nearly 100 swarms lasting 6 months to 7 years that have spatial and temporal patterns consistent with natural fluid injections in the crust.

1. Introduction

Fluid transport in Earth's crust is central to the behavior and evolution of hydrothermal systems (Cox, 2016), the formation of mineral deposits, and groundwater storage. It is of importance for earthquake phenomena at all stages of the seismic cycle (Fialko, 2004; Miller, 2020). Fluid flow is believed to vary with time, as dynamic processes in the Earth can lead to transient changes in permeability (Elkhoury et al., 2006; Manga et al., 2012). Some fluid migration processes are characteristically episodic. Understanding the origins of transient permeability changes, the relevant time scales of these processes, and the distribution of fluid transients in the Earth are fundamental problems in geoscience.

For resolving deep transient flow patterns, direct measurements are the most desirable but are scarce. Geodetic data, while indirect, can be used to infer deeper processes from surface deformation that is sufficiently large (Fialko, 2004; Neal et al., 2019; Sigmundsson et al., 2015). The geological record contains various forms of evidence for the frequent occurrence of transient fluid injection episodes, such as the textures of hydrothermal mineral deposits (Cox, 2016; Sibson, 2020). Another line of evidence for deep transient fluid processes comes from earthquake swarms, which are viewed as a byproduct of aseismic driving processes and therefore an observable marker of them (Hainzl et al., 2013).

The most likely aseismic processes behind swarms are fluid pressure diffusion and aseismic slip (Holtkamp & Brudzinski, 2011; Lohman & McGuire, 2007). These processes explain many distinctive characteristics of swarms, such as migratory behavior, non-stationary temporal patterns, and delayed timing of the largest events (Hainzl et al., 2013; Holtkamp & Brudzinski, 2011; Vidale & Shearer, 2006). The aforementioned characteristics stand in contrast to those of mainshock-aftershock sequences, which are predominantly driven by stress transfer (Dieterich, 1994; Felzer & Brodsky, 2006; Stein, 1999), and have aftershock rates that decay with time. Swarms typically last days to months (Hauksson et al., 2016; Lindenfeld et al., 2012;

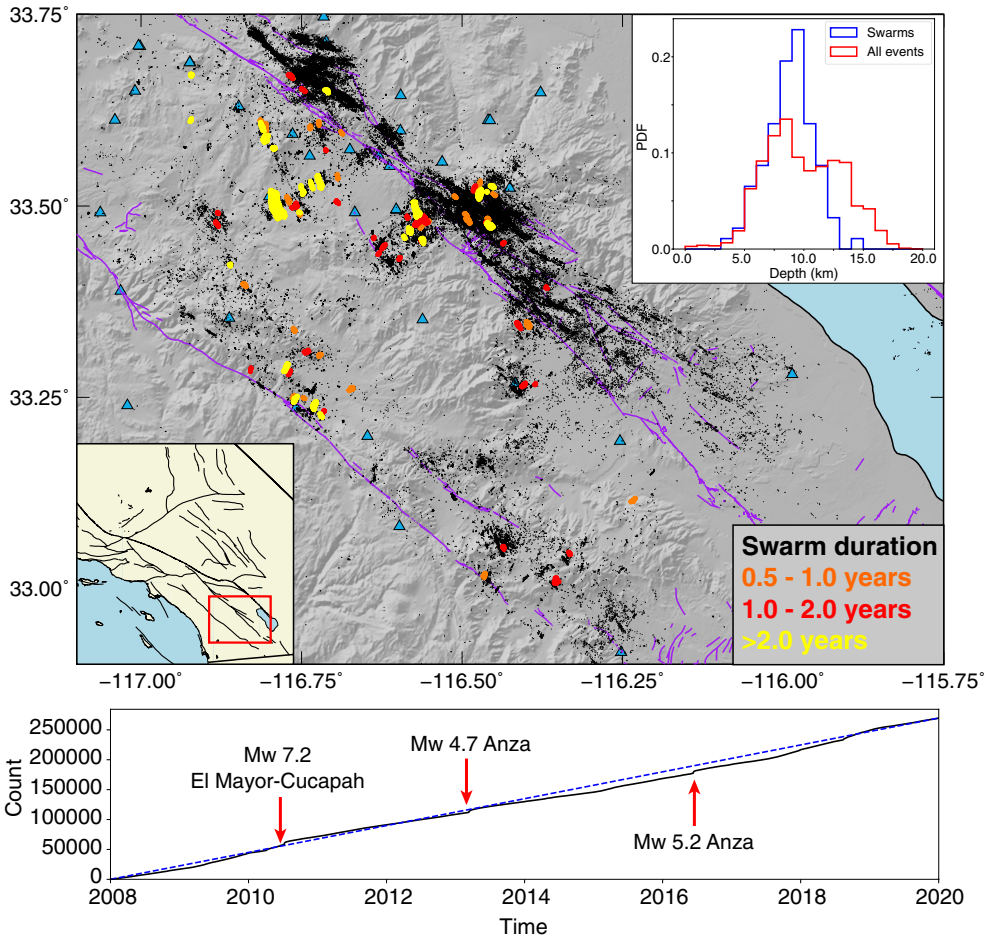

Figure 1. Map of study region and 92 long-duration swarms identified in this study. Swarms are color-coded by duration. Upper right inset shows the depth distribution of cluster centroids compared with regional seismicity depth distribution. Swarm clusters have a narrower depth range. Lower panel shows cumulative number of earthquakes with time, with the blue line indicating the 12-years average rate. The seismicity rate is relatively steady from 2008–2020. Faults from U.S. Geological Survey and California Geological Survey (2004).

Ruhl et al., 2016), but have occasionally been observed to last for years (Kisslinger, 1975; Ross et al., 2020; Thouvenot et al., 2016).

Swarms are common to regions associated with magmatism (Pang et al., 2019; Shelly et al., 2016; Yukutake et al., 2011), rifting (Barros et al., 2020; Duverger et al., 2018; Ibs-von Seht et al., 2008) and hydrothermalism (Enescu et al., 2009). Southern California is a region known for frequent earthquake swarms, with the Salton Trough being an epitome of such activity (Chen & Shearer, 2011; Hauksson et al., 2017, 2013; Johnson & Hadley, 1976; Zaliapin & Ben-Zion, 2013). Other parts of California occasionally are host to swarms, with the 2016–2020 Cahuilla swarm (Ross et al., 2020) being a notable example. This sequence was shown to have likely been driven by natural fluid injection into a fault zone from a deeper reservoir, with the pressure diffusing slowly through the fault over 4 years. The long duration of this sequence, low but steady seismicity rate, and the relatively low heat flow make it appear anomalous with regards to typical views of earthquake swarms.

Following the observations of this unusual sequence, we used deep learning algorithms to build a 12-years high-resolution seismicity catalog to look for additional examples of this activity in Southern California (Figure 1). We found that such multi-year ultra-slowly migrating swarms are not anomalous—but widespread—and were active at all times during the 12-years study period. Many have characteristics of fluid pressure diffusion as the driving process. These observations may indicate that transient fluid injection

processes are an important part of crustal fluid transport in Southern California and, in addition to the hydrogeological importance, such processes have a significant unrecognized impact on regional seismicity patterns.

2. Data

We used EH and HH continuous waveforms provided by the Southern California Seismic Network (SCSN) for the period 2008–2020, which are publicly available from the Southern California Earthquake Data Center (scedc.caltech.edu). In total 99 continuous stations were used (Figure S1). The data were kept at 100 Hz sampling rate.

3. Methods

3.1. Seismicity Catalog Construction

We produced the seismicity catalog in this study from just the raw waveform data. Most steps performed are identical to those described in Ross et al. (2020). The detection portion of the procedure uses two deep learning algorithms sequentially. These steps consist of first detecting earthquakes on individual three-component stations, and then associating these detections across the seismic network to specific event detections. Note that no magnitudes are computed because accurate estimation for very small events is inherently difficult and is not needed for this work.

The phase detection stage uses the trained neural network architecture of Ross et al. (2020) without adjustment, which outputs P- and S-wave probabilities at each time step. We applied this algorithm to the entire 12 years continuous waveform archive to detect P- and S-waves using 16 s seismograms. The data were bandpass filtered 3–20 Hz beforehand. Picks were made by taking the peak sigmoid probability whenever a value of 0.5 was exceeded for either phase type. This led to a database of 7.2 million tentative phase arrivals.

The next step of the procedure utilizes the PhaseLink algorithm (Ross et al., 2019) to associate the phase detections to earthquakes and build an initial catalog. PhaseLink uses a recurrent neural network architecture made of bidirectional Gated Recurrent Units to sequentially predict and link together phase detections (Ross et al., 2019). A synthetic training data set was created for the region shown in Figure S1 by placing synthetic hypocenters randomly throughout the region. This procedure is described in detail in Ross et al. (2019).

There are several hyperparameters associated with the Phase Link detection process, which we describe next. Sequences of 500 picks were processed at a time with a maximum sequence duration of 120 s. These are unchanged from the original paper. We required four phase detections to nucleate a cluster, merged clusters with at least two phase detections in common, and required a minimum of 12 detections left after removing duplicates to retain an event. We tuned these parameters based on random visual inspection of events to ensure the false positive rate was below 1%. In total 323,709 events were detected. Next, we located the events with NonLinLoc, a probabilistic non-linear hypocenter inversion algorithm (Lomax et al., 2000) (Figure S2). We used the 1D velocity model of Hadley and Kanamori (Hadley & Kanamori, 1977) and the equal differential time likelihood function.

The next step involved pairwise event relocation with waveform cross-correlation. We correlated all earthquakes with their nearest 500 neighbors to measure precise differential times. Seismograms were defined using only picks that came out of the associator, starting 0.1 s before the pick. The seismogram windows were 1.1 s long. P-wave correlations were only performed on the vertical component, while S-wave correlations were done on the horizontal components. We band-pass filtered the data between 1 and 15 Hz and required a minimum cross-correlation coefficient of 0.7. This resulted in roughly 245 million differential times. Finally, we relocated the catalog with the GrowClust algorithm (Trugman & Shearer, 2017), a cluster-based double-difference relocation algorithm. Here, we used a minimum r value of 0.7 and required at least eight differential times for relocation. This catalog is the final one produced and is shown in Figure 1.

3.2. Extraction of High-Density Seismicity Clusters

In visually examining the seismicity, a striking feature is that the seismicity often forms very dense clusters ~100–500 m in diameter that are spatially distinct. This observation motivates the usage of a clustering algorithm to extract these dense clusters to study their evolution in space and time. We used the DBSCAN algorithm (Ester et al., 1996) to achieve this, as the algorithm was designed for such density-based clustering tasks. This algorithm has two hyperparameters that control the clustering results: a spherical radius used to search for neighbor points and the minimum number of points within a sphere to grow a cluster. We applied DBSCAN directly to the 3D hypocenters and used a spherical radius of 100 meters, while requiring at least one event to be within the sphere to grow the cluster (the fewest number of events possible in a cluster). Afterward, we only retained clusters with at least 50 events. This results in 255 clusters in total (Figure S3).

The parameters that we used to extract the clusters were chosen after trying a broad range of values and visually examining the results. Since we required only one event to grow a cluster, the only parameter that was tuned was the spherical radius, which was performed with the goal of extracting the ~100–500 m clusters seen visually in the seismicity. When this value was too small, the seismicity clusters that we saw visually in maps were incorrectly split into many smaller ones by DBSCAN. When the value was too large, the many distinct seismicity clusters were erroneously merged into a single cluster by DBSCAN. By using these guiding principles, we ended up at the optimal parameters described above, however we note that there is some tolerance in these values. More importantly, the main conclusions of this study do not depend on these values.

3.3. Swarm Identification

We visually examined all of the 255 clusters and their seismicity rates over 2008–2020 (e.g., Figure 2, and S4). While many of these exhibited steady rates with time, almost half of them displayed non-stationary rates that were primarily in the form of transient episodes of seismic activity lasting months to years. From these observations, we developed a simple automated scheme to extract these transients and their associated events, such that each could be promptly reviewed manually afterward.

The scheme for extracting these transients was designed to identify windows of time for which seismicity rates exceed a background rate by a specified amount. Our procedure is motivated by the short-term average/long-term average (STA/LTA) algorithm for detecting seismic waves (Allen, 1982). For each of the 255 clusters, we first produced a smoothed seismicity rate at daily intervals (Marsan et al., 2013),

$$\mu(t) = \frac{2}{t_b - t_a},$$

where the quantity t_b-t_a represents a window of time containing exactly two events that is centered on t, such that one event is contained in $[t_a, t]$, and another event is contained in $[t, t_b]$. The smoothed rate is then divided by the minimum value observed during the 12 years, which is taken as a reference rate. We chose this because some of the swarms last for 4–7 years, and the average value over the 12-year period is not representative of the activity outside of the swarm. Then, with a simple trigger mechanism, we identify sequences whenever the normalized rate exceeds 20 and triggers off when the normalized rate falls below 10. These parameters were tuned against visual inspection of the results. We only retain swarms that have more than 50 events; while this number could have been lowered somewhat to increase the amount of sequences for study, even with a minimum of 50 there was plenty of data available for analysis, and we felt no need to lower the quality threshold further. Finally, we note for clarity that once the swarms are extracted (the start time, end time, and set of events between them), we no longer use the rate values previously discussed in any of the subsequent analysis.

This process results in 118 candidate swarms lasting at least 6 months. We then manually reviewed each of these and found 92 of these to be genuine swarms based on temporal evolution, lack of rate decay with time, and delayed peak rates after the start of each sequence. The start and end times of each sequence were manually adjusted if the automated algorithm performed poorly at identifying these quantities. These genuine

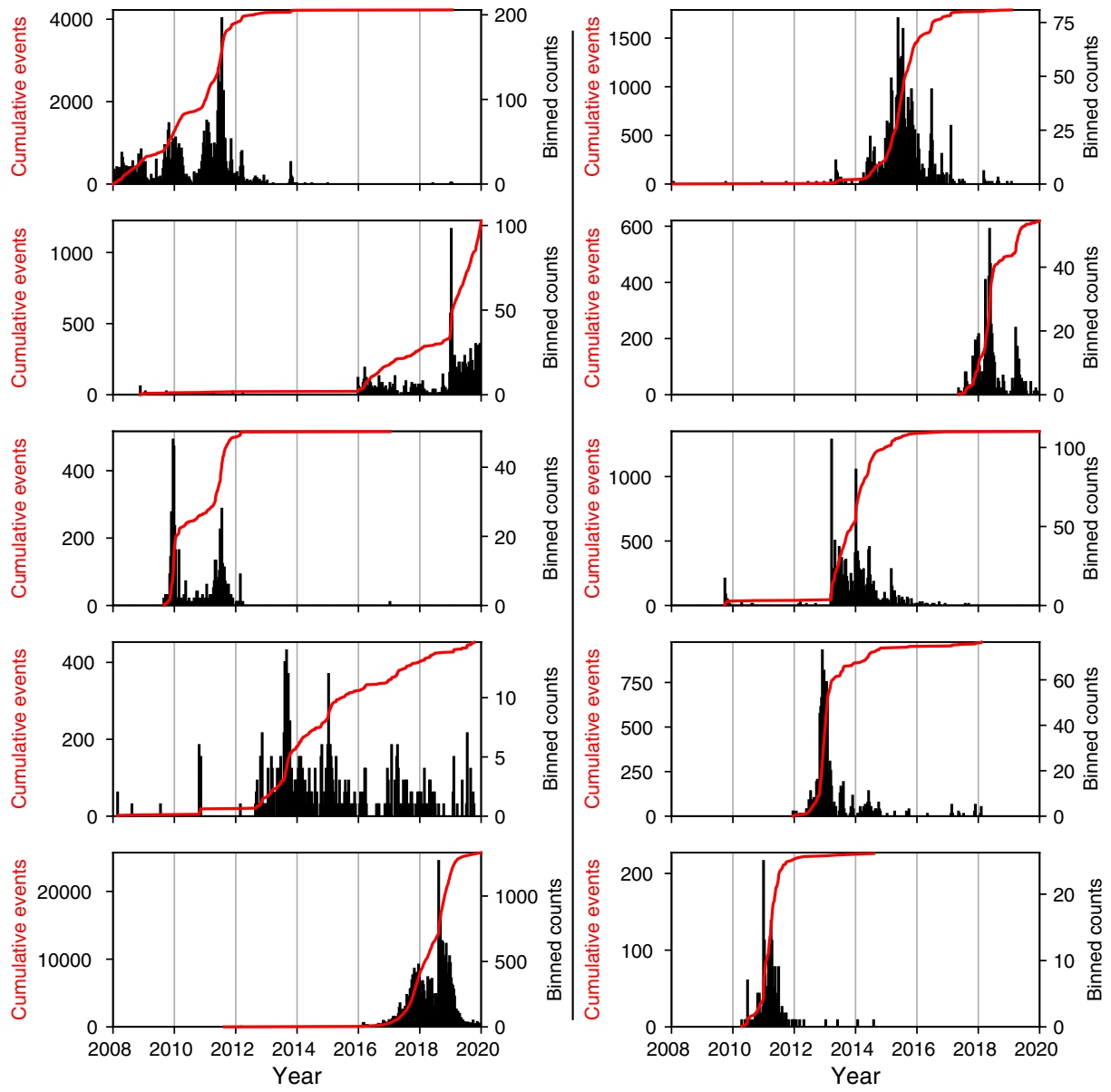

Figure 2. Temporal history of 10 Southern California swarms. Sequences vary in duration from ~2 to 7 years. Swarms generally exhibit initial rate acceleration and eventual rate deceleration, with peak rate typically long after the onset. Overall daily rates are low but sustained for a long time, resulting in significant cumulative activity. Counts are measured in 10-days bins. Bottom left panel shows the 2016–2020 Cahuilla swarm.

swarms were retained for final analysis, as the visual inspection of these results confirmed they were close to what we would have determined manually.

We note that if two spatially disjoint seismicity clusters were active at the same time, perhaps as part of a regional scale aseismic process, our approach may not result in these clusters being merged together. Merging such cases requires making fairly strong assumptions about the spatiotemporal behavior of seismicity, which may be appropriate for short duration sequences but are difficult to justify across the entire catalog for months-to-years long sequences like we are investigating here. As such, we avoid analyses that might be impacted by inadvertently splitting spatially disjoint clusters.

An additional point of importance is that our method was designed to only identify swarms in relatively low background rate areas. Therefore, areas like the San Jacinto fault zone, which has very high seismicity rates, may also have such swarms, but these would be undetected by our approach; targeting these may be

the subject of future work. We have therefore limited our analysis to interpreting the spatial distribution of swarms where they are observed, and do not comment about what may be happening in regions where they are absent.

4. Results

Figure 1 presents the relocated seismicity catalog for the study area, which focuses mainly on the region bounded by the San Jacinto and Elsinore fault zones. The regional geology is largely crystalline rocks of the Peninsular Ranges (Jennings et al., 1977), with low-to-average heat flow (Hauksson, 2011) (<75 mW/m^2). This area is very active seismically, having produced about 20% of all earthquakes listed in the regional Southern California Seismic Network catalog from 1981–2020, despite no event being larger than M 5.4. We focus our analysis on spatially dense seismicity clusters, which are defined using a density-based clustering algorithm (see methods). The clusters contain at least 50 events, and most are about a few hundred meters in size. Examples of these clusters are shown in Figure 1, with the full set obtained shown in Supplementary Figure 3.

The aggregate regional seismicity rate is remarkably steady from 2008 to 2020 (Figure 1); however, when considering the dense clusters individually, the seismicity rate is often highly non-stationary. Ten examples are shown in Figure 2, with an additional 10 shown in Supplementary Figure 4. In each case, we observe that the seismic activity grows rapidly from virtually zero prior activity. Then, following a period of increased seismicity the cluster's activity diminishes. Using these time points, we infer that the transient episodes in Figure 2 range from 2 to 7 years in duration. Each swarm shown in Figure 2 would rank among the longest previously documented—not just in Southern California—but globally; for example, the 1965–1967 Matsushiro, Japan swarm, the Ubaye, France swarms of 2003–2004 and 2012–2015 (Jenatton et al., 2007; Thouvenot et al., 2016) and the 2008–2020 Cahuilla, USA swarm (Ross et al., 2020). Furthermore, there is concurrency between several of them.

The time history of these transient episodes does not follow a single simple Omori law (Utsu et al., 1995), which says that the rate of events decreases as t^{-1} and is a key differentiator of aftershock sequences from swarms. We find the peak event rate is significantly delayed (~months to years) after the onset of activity (Figure 2 and S4). The sequence shown in the bottom left panel of Figure 2 is the previously mentioned 2016–2020 Cahuilla swarm (Ross et al., 2020). The other swarms shown bear several similarities to the Cahuilla swarm, with more than half of them slowly accelerating to a relatively steady rate before decelerating to a complete shutoff. While the swarms are active, some exhibit multiple cycles of acceleration and deceleration, which could be related to slow slip transients (Bourouis & Bernard, 2007; Zhu et al., 2020). These characteristics may be useful observational constraints for modeling these sequences.

The seismicity rates during these swarms are relatively low compared to most documented in the literature (Thouvenot et al., 2016; Vidale & Shearer, 2006) and, of those shown in Figure 2, the Cahuilla swarm is by far the most active; the rates for the other swarms are much lower. It is only by considering the spatio-temporal characteristics of the activity that it is apparent that these events are not simply background tectonic events.

The swarms in Figure 2 are only a fraction of those identified with this behavior. To get a sense for their geographical distribution, Figure 1 shows all clusters that contain least one swarm lasting 6 months or more that meet a set of basic criteria (see methods). While even shorter swarms may indeed be occurring, our focus here is on longer sequences that have previously been considered rare or anomalous. In total there are 92 long swarms shown and colored according to their duration. Of these, 36 have durations between 1 and 2 years, and 28 are two years or longer. These sequences lack a clear Omori decay, often exhibit spatial migration with time, and have anomalously long durations as compared with the largest magnitude event. The long duration swarms are widespread over the study area, despite the low-to-average heat flow (Hauksson, 2011). There is no regional evidence for massive CO_2 degassing, as seen where other long duration swarms (months-to-years long) have been identified, such as the Eger rift in the Czech Republic (Bräuer et al., 2009) or the Italian Apennines (Miller et al., 2004).

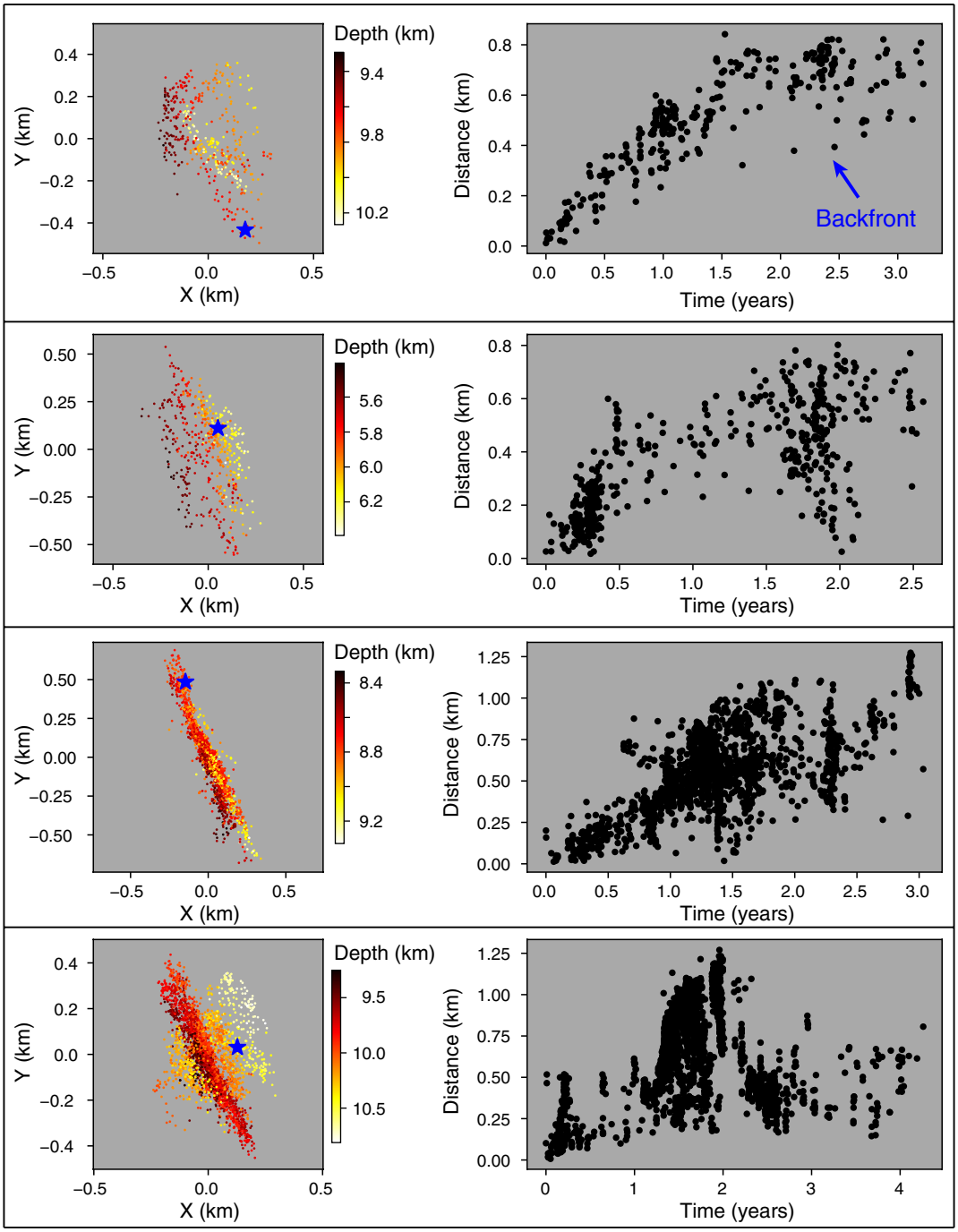

Figure 3. Diversity of seismicity migration in swarms. Left: map view of each swarm cluster colored by depth. Blue star indicates estimate of the location of the sequence origin based on the earliest events in the swarm. Right: radial distance of seismicity relative to blue star. Sequences exhibit very slow migration fronts away from origin, as well as migration backfronts, suggestive of natural fluid injection. These fault zones are inferred to have a permeability of $\sim 10^{-17}$–10^{-18} m^2.

From visual inspection, 49 of the 92 swarms (53%) shown in Figure 1 exhibit prominent migration behavior, and four exemplary cases are shown in Figure 3; these are accompanied by plots of the seismicity in map view. Using the earliest events in each swarm as a reference point, the swarms expand outward and away from this origin. These sequences demonstrate considerable diversity in their migration behavior. Their durations vary from 2.5 to 4 years. The migration velocities are extremely slow, ranging from about 0.5 to

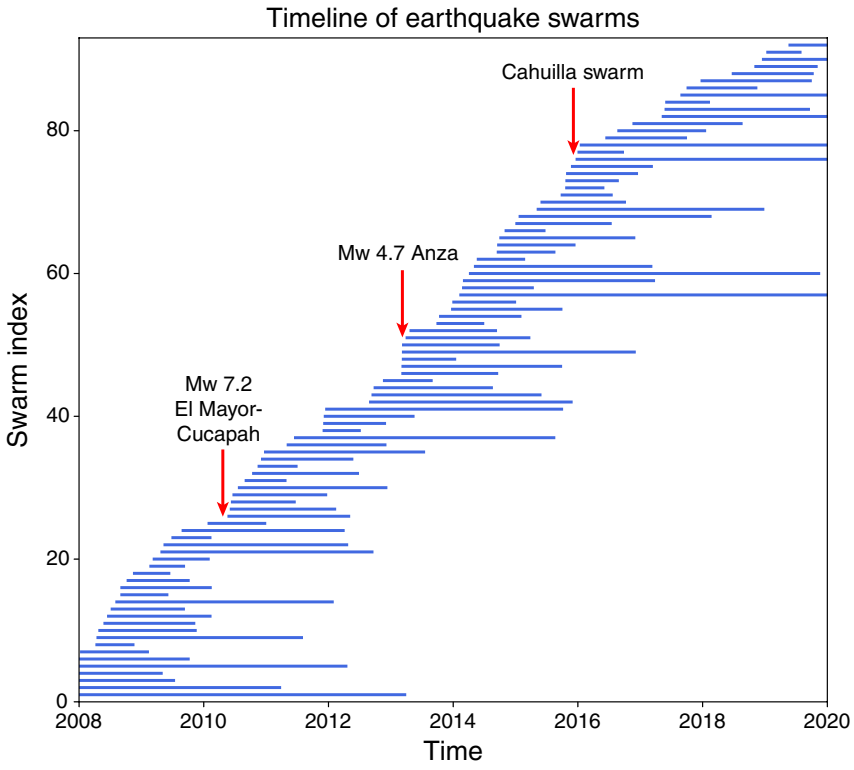

Figure 4. Chronology of swarms for the period 2008–2020. Sequences are sorted by inferred start time. Shorter swarms are much more frequent than longer swarms. There is always at least one swarm active during the 12-year period.

1.5 m/day. Many of the sequences have a visible backfront to the diffusion, where events near the injection point cease but activity continues at greater distances (Parotidis et al., 2004, 2005). Together, these characteristics suggest that the swarms were driven by natural fluid injection (Cox, 2016; Ross et al., 2020). We estimate the diffusivities of the swarms in Figure 3 to be 0.03–0.05 m^2/s based on the rate of radial expansion with time (Shapiro et al., 1997). Following the approach of Ross et al. (2020) and the values therein, we find the permeabilities of the faults here to be $\sim 10^{-17}$–10^{-18} m^2. This is in contrast to permeabilities of $\sim 10^{-11}$–10^{-15} m^2 reported for other migrating earthquake sequences (Cappa et al., 2009; Miller, 2020). It is unclear whether the swarms without a clear diffusion pattern represent genuine differences in the sequence behavior or result from data limitations.

During a fluid injection transient, the backfront is related to the shutdown of the injection, which can provide constraints on the duration of the injection process (Segall & Lu, 2015). For the swarms shown, the injection process appears to last on the order of several months. As the duration of the swarm activity is substantially longer, these observations suggest that the fluid injection source has a protracted impact (for potentially years afterward), as fluid pressure continues to diffuse through the fault zone long after the source shuts down.

As hinted at by the examples in Figure 2, there is concurrency among the individual episodes. With the 92 long swarms identified (Figure 1), it is natural to ask about their regional chronology, as this can provide greater context for the underlying aseismic processes and their importance. This is shown in Figure 4, where each row represents a different swarm, and the collection of swarms is sorted by the time at which each begins.

It is also of interest to examine the depth distribution of these swarms in comparison to the overall seismicity distribution (Figure 1, inset). While the depth range over the whole region is relatively broad (~5–17 km), the centroid depths of the swarm clusters have a fairly narrow distribution (5–11 km). This may suggest that the causative processes are associated with properties of this particular depth range, although it is outside the scope of this work to identify those processes.

There are several important aspects that are worth discussing in detail. First, the swarms are clearly transient and range in duration from 6 months to 7 years. Shorter swarms are more frequent than longer swarms. Second, there is a swarm active somewhere at all times during the 12-year period, which implies the driving processes are always present in this region. Finally, while the longer duration swarms are less frequent, there is nearly always one or more long swarm active during the 12-year period. If these swarms are predominantly driven by fluid pressure diffusion, then these transients likely represent a critical mechanism for fluid transport deep in the crust. Other fluid diffusion transients could be occurring, but without producing any, or only limited, seismicity and therefore not documented here.

5. Discussion

We have identified nearly a hundred swarms lasting months to years in an active portion of the Southern California plate boundary not typically associated with this type of activity. Our observations do not exclude the possibility of even longer swarms, which would not have been identified by the methods and data utilized. Many of the swarms exhibit very slow diffusive behavior away from a common origin and prominent migration backfronts, which likely is the byproduct of natural fluid injection into fault zones (Ross et al., 2020); a small fraction of swarms (~3 sequences) however have distinctly different behavior, with faster migration velocities and linear migration patterns, and may have been driven by aseismic slip events instead (Chen et al., 2012; Lohman & McGuire, 2007). The combined observations of long swarm duration, low but sustained seismicity rates, and relatively low regional heat flow would make any one of these sequences an anomaly by standard views of earthquake swarms. The fact that nearly a hundred have occurred in a 12-year period implies that this definition should be broadened.

Such long-duration swarms may have evaded prior detection in part because previous studies have used expectations of swarm behavior to define search criteria that would preclude their detection (Chen et al., 2012; Holtkamp & Brudzinski, 2011; Vidale & Shearer, 2006; Zaliapin & Ben-Zion, 2013). The much more detailed seismicity catalog also provides a more expansive view of these sequences. A consequence of the swarms being previously unidentified is that studies would have assumed the bulk of these events were background seismicity within a highly active tectonic region (Mueller, 2019; Powers & Field, 2013; Richards-Dinger & Dieterich, 2012). Characterizing these events instead as part of swarms has important implications for seismic hazard because the seismicity rates are highly non-stationary with time, and the maximum magnitudes for swarms may be different than those assumed for tectonic event sequences. We find that 26.4% (56,823) of the events in the relocated catalog occurred as part of these swarms. This is all the more remarkable given that the study area includes the central San Jacinto fault zone, which is the most active part of southern California (Ross et al., 2017). Applying a broader definition of swarms to other active tectonic regions may lead to similar findings.

By interpreting these swarms as primarily a manifestation of transient fluid injection processes, the observation that one or more episodes was active at all times during the 12-years study period implies that this physical mechanism is of broad regional importance for crustal fluid transport. This type of process is consistent with fault valving (Cox, 2016; Sibson, 1981, 2020) and envisions episodic fluid injection into a fault zone from a deeper natural reservoir. In this model the reservoir is initially sealed off from the fault zone, perhaps due to mineralization (Cox, 2016), but somehow the seal breaks, resulting in overpressured fluids being injected into the fault. Eventually the fault zone seals itself and the whole cycle repeats while pressure builds back up. Fault valving can result in large fluid fluxes being transmitted through a fault zone episodically and has been suggested to be responsible for creating fault-zone-hosted mineral deposits (Sibson, 2020). The 2016–2020 Cahuilla swarm itself is strong evidence for fault valving in situ (Ross et al., 2020), and many of the swarms observed in this study have very similar evolutionary characteristics. The origin of these fluids may be related to dehydration reactions (Hacker, 1997; Sibson, 2020) or influx of mantle fluids (Kennedy et al., 1997).

The results of this study were aided by the use of a clustering algorithm to break up the seismicity into spatially disjoint clusters and an automated method for estimating the swarm's temporal extent. While the parameters of these algorithms can affect the obtained set of clusters and swarms, the widespread existence

of these ultra-slow sequences, diffusive migration patterns over several years' time, and their occurrence at all times throughout the 12-years study period do not depend on such parameters.

When considering these fluid injection processes together with the complex surrounding fault zones, a picture emerges of southern California as a dynamic plate boundary environment not dominated by a single process. Tectonic loading contributes to substantial regional seismicity, producing occasional moderate to large events and considerable clustering, while fluid injection episodes are steadily occurring throughout the region and compounding the total seismic activity with ultra-slow migratory earthquake swarms.

Data Availability Statement

All data used are publicly available from the Southern California Earthquake Data Center (scedc.caltech.edu). The developed catalog will also be publicly hosted at the SCEDC.

Acknowledgments
The authors thank Andrea Llenos, Clara Yoon, Stephen Miller, and Pascal Bernard for reviewing the paper. The authors also thank Jonathan Smith for helpful comments on the initial manuscript. This study was supported by the National Science Foundation under award EAR-2034167.

References

Allen, R. (1982). Automatic phase pickers: Their present use and future prospects. *Bulletin of the Seismological Society of America*, *72*(6B), S225–S242.

Barros, L. D., Cappa, F., Deschamps, A., & Dublanchet, P. (2020). Imbricated aseismic slip and fluid diffusion drive a seismic swarm in the Corinth Gulf, Greece. *Geophysical Research Letters*, *47*(9), e2020GL087142. https://doi.org/10.1029/2020GL087142

Bourouis, S., & Bernard, P. (2007). Evidence for coupled seismic and aseismic fault slip during water injection in the geothermal site of Soultz (France), and implications for seismogenic transients. *Geophysical Journal International*, *169*(2), 723–732. https://doi.org/10.1111/j.1365-246X.2006.03325.x

Bräuer, K., Kämpf, H., & Strauch, G. (2009). Earthquake swarms in non-volcanic regions: What fluids have to say? *Geophysical Research Letters*, *36*(17), L17309. https://doi.org/10.1029/2009GL039615

Cappa, F., Rutqvist, J., & Yamamoto, K. (2009). Modeling crustal deformation and rupture processes related to upwelling of deep CO2-rich fluids during the 1965–1967 Matsushiro earthquake swarm in Japan. *Journal of Geophysical Research*, *114*(B10). https://doi.org/10.1029/2009JB006398

Chen, X., & Shearer, P. M. (2011). Comprehensive analysis of earthquake source spectra and swarms in the Salton Trough, California. *Journal of Geophysical Research*, *116*(B9). https://doi.org/10.1029/2011JB008263

Chen, X., Shearer, P. M., & Abercrombie, R. E. (2012). Spatial migration of earthquakes within seismic clusters in Southern California: Evidence for fluid diffusion. *Journal of Geophysical Research*, *117*(B4), B04301. https://doi.org/10.1029/2011JB008973

Cox, S. F. (2016). Injection-driven swarm seismicity and permeability enhancement: Implications for the dynamics of hydrothermal ore systems in high fluid-flux, overpressured faulting regimes—an invited paper. *Economic Geology*, *111*(3), 559–587. https://doi.org/10.2113/econgeo.111.3.559

Dieterich, J. (1994). A constitutive law for rate of earthquake production and its application to earthquake clustering. *Journal of Geophysical Research*, *99*(B2), 2601–2618. https://doi.org/10.1029/93JB02581

Duverger, C., Lambotte, S., Bernard, P., Lyon-Caen, H., Deschamps, A., & Nercessian, A. (2018). Dynamics of microseismicity and its relationship with the active structures in the western Corinth Rift (Greece). *Geophysical Journal International*, *215*(1), 196–221. https://doi.org/10.1093/gji/ggy264

Elkhoury, J. E., Brodsky, E. E., & Agnew, D. C. (2006). Seismic waves increase permeability. *Nature*, *441*(7097), 1135–1138. https://doi.org/10.1038/nature04798

Enescu, B., Hainzl, S., & Ben-Zion, Y. (2009). Correlations of seismicity patterns in Southern California with surface heat flow data correlations of seismicity patterns in Southern California with surface heat flow data. *Bulletin of the Seismological Society of America*, *99*(6), 3114–3123. https://doi.org/10.1785/0120080038

Ester, M., Kriegel, H.-P., Sander, J., & Xu, X. (1996). A density-based algorithm for discovering clusters in large spatial databases with noise (Vol. 96, pp. 226–231). Presented at the Kdd

Felzer, K. R., & Brodsky, E. E. (2006). Decay of aftershock density with distance indicates triggering by dynamic stress. *Nature*, *441*(7094), 735–738. https://doi.org/10.1038/nature04799

Fialko, Y. (2004). Evidence of fluid-filled upper crust from observations of postseismic deformation due to the 1992 Mw7.3 Landers earthquake. *Journal of Geophysical Research*, *109*(B8). https://doi.org/10.1029/2004JB002985

Hacker, B. R. (1997). Diagenesis and fault valve seismicity of crustal faults. *Journal of Geophysical Research*, *102*(B11), 24459–24467. https://doi.org/10.1029/97JB02025

Hadley, D., & Kanamori, H. (1977). Seismic structure of the Transverse Ranges, California. *GSA Bulletin*, *88*(10), 1469–1478. https://doi.org/10.1130/0016-7606(1977)88<1469:SSOTTR>2.0.CO;2

Hainzl, S., Zakharova, O., & Marsan, D. (2013). Impact of aseismic transients on the estimation of aftershock productivity parameters. *Bulletin of the Seismological Society of America*, *103*(3), 1723–1732. https://doi.org/10.1785/0120120247

Hauksson, E. (2011). Crustal geophysics and seismicity in southern California. *Geophysical Journal International*, *186*(1), 82–98. https://doi.org/10.1111/j.1365-246X.2011.05042.x

Hauksson, E., Andrews, J., Plesch, A., Shaw, J. H., & Shelly, D. R. (2016). The 2015 Fillmore earthquake swarm and possible crustal deformation mechanisms near the Bottom of the Eastern Ventura Basin, California. *Seismological Research Letters*, *87*(4), 807–815. https://doi.org/10.1785/0220160020

Hauksson, E., Meier, M., Ross, Z. E., & Jones, L. M. (2017). Evolution of seismicity near the southernmost terminus of the San Andreas Fault: Implications of recent earthquake clusters for earthquake risk in southern California. *Geophysical Research Letters*, *44*(3), 1293–1301. https://doi.org/10.1002/2016gl072026

Hauksson, E., Stock, J., Bilham, R., Boese, M., Chen, X., Fielding, E. J., et al. (2013). Report on the August 2012 Brawley earthquake swarm in Imperial Valley, Southern California. *Seismological Research Letters*, *84*(2), 177–189. https://doi.org/10.1785/0220120169

Holtkamp, S. G., & Brudzinski, M. R. (2011). Earthquake swarms in circum-Pacific subduction zones. *Earth and Planetary Science Letters*, *305*(1), 215–225. https://doi.org/10.1016/j.epsl.2011.03.004

Ibs-von Seht, M., Plenefisch, T., & Klinge, K. (2008). Earthquake swarms in continental rifts — A comparison of selected cases in America, Africa and Europe. *Tectonophysics*, *452*(1), 66–77. https://doi.org/10.1016/j.tecto.2008.02.008

Jenatton, L., Guiguet, R., Thouvenot, F., & Daix, N. (2007). The 16,000-event 2003–2004 earthquake swarm in Ubaye (French Alps). *Journal of Geophysical Research*, *112*(B11), B11304. https://doi.org/10.1029/2006JB004878

Jennings, C. W., Strand, R. G., & Rogers, T. H. (1977). Geologic map of California: California Division of Mines and Geology, scale 1: 750,000.

Johnson, C. E., & Hadley, D. M. (1976). Tectonic implications of the Brawley earthquake swarm, Imperial Valley, California, January 1975. *Bulletin of the Seismological Society of America*, *66*(4), 1133–1144.

Kennedy, B. M., Kharaka, Y. K., Evans, W. C., Ellwood, A., DePaolo, D. J., Thordsen, J., et al. (1997). Mantle fluids in the San Andreas Fault System, California. *Science*, *278*(5341), 1278–1281. https://doi.org/10.1126/science.278.5341.1278

Kisslinger, C. (1975). Processes during the Matsushiro, Japan, Earthquake swarm as revealed by leveling, gravity, and spring-flow observations. *Geology*, *3*(2), 57–62. https://doi.org/10.1130/0091-7613(1975)3<57:PDTMJE>2.0.CO;2

Lindenfeld, M., Rümpker, G., Link, K., Koehn, D., & Batte, A. (2012). Fluid-triggered earthquake swarms in the Rwenzori region, East African Rift—Evidence for rift initiation. *Tectonophysics*, *566–567*, 95–104. https://doi.org/10.1016/j.tecto.2012.07.010

Lohman, R. B., & McGuire, J. J. (2007). Earthquake swarms driven by aseismic creep in the Salton Trough, California. *Journal of Geophysical Research*, *112*(B4), B04405. https://doi.org/10.1029/2006JB004596

Lomax, A., Virieux, J., Volant, P., & Berge-Thierry, C. (2000). Probabilistic Earthquake location in 3D and layered models. In C. H. Thurber, & N. Rabinowitz (Eds.), *Advances in seismic event location* (pp. 101–134). Springer Netherlands. https://doi.org/10.1007/978-94-015-9536-0_5

Manga, M., Beresnev, I., Brodsky, E. E., Elkhoury, J. E., Elsworth, D., Ingebritsen, S. E., et al. (2012). Changes in permeability caused by transient stresses: Field observations, experiments, and mechanisms. *Reviews of Geophysics*, *50*(2). https://doi.org/10.1029/2011RG000382

Marsan, D., Prono, E., & Helmstetter, A. (2013). Monitoring aseismic forcing in fault zones using earthquake time series. *Bulletin of the Seismological Society of America*, *103*(1), 169–179. https://doi.org/10.1785/0120110304

Miller, S. A. (2020). Aftershocks are fluid-driven and decay rates controlled by permeability dynamics. *Nature Communications*, *11*(1), 5787. https://doi.org/10.1038/s41467-020-19590-3

Miller, S. A., Collettini, C., Chiaraluce, L., Cocco, M., Barchi, M., & Kaus, B. J. P. (2004). Aftershocks driven by a high-pressure CO2 source at depth. *Nature*, *427*(6976), 724–727. https://doi.org/10.1038/nature02251

Mueller, C. S. (2019). Earthquake catalogs for the USGS National Seismic Hazard Maps. *Seismological Research Letters*, *90*(1), 251–261. https://doi.org/10.1785/0220170108

Neal, C. A., Brantley, S. R., Antolik, L., Babb, J. L., Burgess, M., Calles, K., et al. (2019). The 2018 rift eruption and summit collapse of Kīlauea Volcano. *Science*, *363*(6425), 367–374. https://doi.org/10.1126/science.aav7046

Pang, G., Koper, K. D., Hale, J. M., Burlacu, R., Farrell, J., & Smith, R. B. (2019). The 2017–2018 Maple Creek Earthquake Sequence in Yellowstone National Park, USA. *Geophysical Research Letters*, *46*(9), 4653–4663. https://doi.org/10.1029/2019GL082376

Parotidis, M., Shapiro, S. A., & Rothert, E. (2004). Back front of seismicity induced after termination of borehole fluid injection. *Geophysical Research Letters*, *31*(2), L02612.

Parotidis, M., Shapiro, S. A., & Rothert, E. (2005). Evidence for triggering of the Vogtland swarms 2000 by pore pressure diffusion. *Journal of Geophysical Research: Solid Earth*, *110*(B5), B05S10.

Powers, P. M., & Field, E. H. (2013). Appendix O: Gridded seismicity sources. *U.S. Geol. Surv. Open-File Rept. 2013-1165-O and California Geol. Surv. Special Rept. 228-O*.

Richards-Dinger, K., & Dieterich, J. H. (2012). RSQSim Earthquake Simulator. *Seismological Research Letters*, *83*(6), 983–990. https://doi.org/10.1785/0220120105

Ross, Z. E., Cochran, E. S., Trugman, D. T., & Smith, J. D. (2020). 3D fault architecture controls the dynamism of earthquake swarms. *Science*, *368*(6497), 1357–1361. https://doi.org/10.1126/science.abb0779

Ross, Z. E., Hauksson, E., & Ben-Zion, Y. (2017). Abundant off-fault seismicity and orthogonal structures in the San Jacinto fault zone. *Science Advances*, *3*(3), 8. https://doi.org/10.1126/sciadv.1601946

Ross, Z. E., Yue, Y., Meier, M.-A., Hauksson, E., & Heaton, T. H. (2019). Phase Link: A deep learning approach to seismic phase association. *Journal of Geophysical Research: Solid Earth*, *124*(1), 856–869. https://doi.org/10.1029/2018JB016674

Ruhl, C. J., Abercrombie, R. E., Smith, K. D., & Zaliapin, I. (2016). Complex spatiotemporal evolution of the 2008 Mw 4.9 Mogul earthquake swarm (Reno, Nevada): Interplay of fluid and faulting. *Journal of Geophysical Research: Solid Earth*, *121*(11), 8196–8216. https://doi.org/10.1002/2016JB013399

Segall, P., & Lu, S. (2015). Injection-induced seismicity: Poroelastic and earthquake nucleation effects. *Journal of Geophysical Research: Solid Earth*, *120*(7), 5082–5103. https://doi.org/10.1002/2015JB012060

Shapiro, S. A., Huenges, E., & Borm, G. (1997). Estimating the crust permeability from fluid-injection-induced seismic emission at the KTB site. *Geophysical Journal International*, *131*(2), F15–F18. https://doi.org/10.1111/j.1365-246X.1997.tb01215.x

Shelly, D. R., Ellsworth, W. L., & Hill, D. P. (2016). Fluid-faulting evolution in high definition: Connecting fault structure and frequency-magnitude variations during the 2014 Long Valley Caldera, California, earthquake swarm. *Journal of Geophysical Research: Solid Earth*, *121*(3), 1776–1795. https://doi.org/10.1002/2015JB012719

Sibson, R. H. (1981). Fluid flow accompanying faulting: Field evidence and models. In *Earthquake prediction* (pp. 593–603). American Geophysical Union (AGU). https://doi.org/10.1029/ME004p0593

Sibson, R. H. (2020). Preparation zones for large crustal earthquakes consequent on fault-valve action. *Earth Planets and Space*, *72*(1), 31. https://doi.org/10.1186/s40623-020-01153-x

Sigmundsson, F., Hooper, A., Hreinsdóttir, S., Vogfjörd, K. S., Ófeigsson, B. G., Heimisson, E. R., et al. (2015). Segmented lateral dyke growth in a rifting event at Bárðarbunga volcanic system, Iceland. *Nature*, *517*(7533), 191–195. https://doi.org/10.1038/nature14111

Stein, R. S. (1999). The role of stress transfer in earthquake occurrence. *Nature*, *402*(6762), 605–609. https://doi.org/10.1038/45144

Thouvenot, F., Jenatton, L., Scafidi, D., Turino, C., Potin, B., & Ferretti, G. (2016). Encore Ubaye: Earthquake swarms, foreshocks, and aftershocks in the Southern French Alps. *Bulletin of the Seismological Society of America*, *106*(5), 2244–2257. https://doi.org/10.1785/0120150249

Trugman, D. T., & Shearer, P. M. (2017). Grow clust: A hierarchical clustering algorithm for relative earthquake relocation, with application to the Spanish springs and Sheldon, Nevada, Earthquake Sequences. *Seismological Research Letters*, *88*(2A), 379–391. https://doi.org/10.1785/0220160188

U.S. Geological Survey, & California Geological Survey. (2004). *Quaternary Fault and Fold Database for the Nation* (Report No. 2004–3033, Version 1.0). https://doi.org/10.3133/fs20043033

Utsu, T., Ogata, Y., S, R., & Matsu'ura (1995). The centenary of the Omori Formula for a Decay Law of aftershock activity. *Journal of Physics of the Earth*, *43*(1), 1–33. https://doi.org/10.4294/jpe1952.43.1

Vidale, J. E., & Shearer, P. M. (2006). A survey of 71 earthquake bursts across southern California: Exploring the role of pore fluid pressure fluctuations and aseismic slip as drivers. *Journal of Geophysical Research*, *111*(B5), B05312. https://doi.org/10.1029/2005jb004034

Yukutake, Y., Ito, H., Honda, R., Harada, M., Tanada, T., & Yoshida, A. (2011). Fluid-induced swarm earthquake sequence revealed by precisely determined hypocenters and focal mechanisms in the 2009 activity at Hakone volcano, Japan. *Journal of Geophysical Research*, *116*(B4), B04308. https://doi.org/10.1029/2010JB008036

Zaliapin, I., & Ben-Zion, Y. (2013). Earthquake clusters in southern California II: Classification and relation to physical properties of the crust. *Journal of Geophysical Research: Solid Earth*, *118*(6), 2865–2877. https://doi.org/10.1002/jgrb.50178

Zhu, W., Allison, K. L., Dunham, E. M., & Yang, Y. (2020). Fault valving and pore pressure evolution in simulations of earthquake sequences and aseismic slip. *Nature Communications*, *11*(1), 4833. https://doi.org/10.1038/s41467-020-18598-z